27. T. N. Titus, H. H. Kieffer, P. R. Christensen, *Science* **299**, 1048 (2002).
28. S. H. Williams, J. R. Zimbelman, *Geology* **22**, 107 (1994).
29. S. W. Ruff *et al.*, *J. Geophys. Res.* **106**, 23921 (2001).
30. H. Y. McSween Jr. *et al.*, *J. Geophys. Res.* **104**, 8679 (1999).
31. J. F. Bell III *et al.*, *J. Geophys. Res* **105**, 1721 (2000).
32. A. R. Gillespie, A. B. Kahle, R. E. Walker, *Remote Sensing Environ.* **20**, 209 (1986).
33. We would like to sincerely thank all those at Raytheon Santa Barbara Remote Sensing who built the THEMIS instrument, and those at the NASA Jet Propulsion Laboratory, Lockheed Martin Astronautics, and Arizona State University, who built and operate the Odyssey spacecraft. This work was supported by the NASA Mars Odyssey Flight Project.

Supporting Online Material
www.sciencemag.org/cgi/content/full/1080885/DC1
SOM Text
Figs. S1 to S5

26 November 2002; accepted 14 May 2003
Published online 5 June 2003;
10.1126/science.1080885
Include this information when citing this paper.

Myosin V Walks Hand-Over-Hand: Single Fluorophore Imaging with 1.5-nm Localization

Ahmet Yildiz,[1] Joseph N. Forkey,[3] Sean A. McKinney,[1,2] Taekjip Ha,[1,2] Yale E. Goldman,[3] Paul R. Selvin[1,2]*

Myosin V is a dimeric molecular motor that moves processively on actin, with the center of mass moving ~37 nanometers for each adenosine triphosphate hydrolyzed. We have labeled myosin V with a single fluorophore at different positions in the light-chain domain and measured the step size with a standard deviation of <1.5 nanometers, with 0.5-second temporal resolution, and observation times of minutes. The step size alternates between 37 + 2x nm and 37 – 2x, where x is the distance along the direction of motion between the dye and the midpoint between the two heads. These results strongly support a hand-over-hand model of motility, not an inchworm model.

Myosin V is a cargo-carrying processive motor that takes ~37-nm center of mass steps along actin filaments (*1*–*3*). Defects in this protein lead to immunological and neurological diseases (*4*). Like many other processive motors, it has two heads held together by a coiled-coil stalk (Fig. 1). Each head of myosin V contains a catalytic domain responsible for actin binding and ATP hydrolysis and a light chain–binding domain that likely acts as a lever arm to amplify small nucleotide-dependent conformational changes in the catalytic domain (*3*, *5*, *6*).

How the two heads of myosin V are coordinated to produce steps is a central, unresolved question. Biochemical and biophysical studies (*3*, *6*, *7*) suggest a hand-over-hand "walking" model in which the two heads alternate in the lead (Fig. 1, left). Another possibility is the so-called "inchworm" model in which one head always leads (Fig. 1, right). A biophysical study of kinesin, another processive motor, concluded an inchworm model was more likely, although it could not rule out an asymmetric type hand-over-hand mechanism (*8*).

The hand-over-hand and inchworm models make different, testable predictions for the motions of each individual head (Fig. 1). For example, the inchworm model predicts that the step size of each catalytic domain is equal to the step size of the stalk [35 to 40 nm (*9*, *10*) or ~37 nm]. In contrast, the hand-over-hand model predicts that the trailing catalytic domain takes a step that is twice the step size of the stalk while the leading catalytic domain does not move. For a single fluorophore attached to the light chain domain of myosin V, the inchworm model predicts a uniform step size of 37 nm, whereas the hand-over-hand model predicts alternating steps of 37 – 2x, 37 + 2x, where x is the in-plane distance of the dye from the midpoint of the myosin (Fig. 1).

To test these models, we have developed a single molecule fluorescence imaging technique capable of locating a single molecule in two dimensions to within 1.5 nm, with subsecond temporal resolution and with a photostability that allows observation for several minutes. Total internal reflection epifluorescence microscopy (TIRF) (*11*–*13*) was used to excite and image many individual fluorophores onto a slow-scan back-thinned charge-coupled device (CCD) with frame-transfer capability, enabling acquisition of multiple sequential images with no interframe deadtime (*14*). Our technique [fluorescence imaging with one-nanometer accuracy (FIONA)] is a 20-fold improvement in the localization accuracy of single fluorophores at room temperature using wide-field methods (*15*, *16*) and a ~10-fold improvement in photostability. Scanning confocal microscopy methods using two nanocrystals of different emission wavelengths have previously achieved a precision of ±6 nm with a total integration time of 20 s (*17*). Fluorescence (*18*) and scattering (*19*) from large (30 and 150 nm, respectively) beads have achieved ~2-nm localization within unspecified time resolution and 30 ms, respectively.

FIONA. A single fluorescent molecule forms a diffraction-limited image of width ≈ λ/2 N.A., or ≈ 250 nm for visible light, where N.A. is the numerical aperture of the collection lens. The center of the image, which, under appropriate conditions, corresponds to the position of the dye, can be located to arbitrarily high precision by collecting a sufficient number of photons. Our method for determining the center relies on

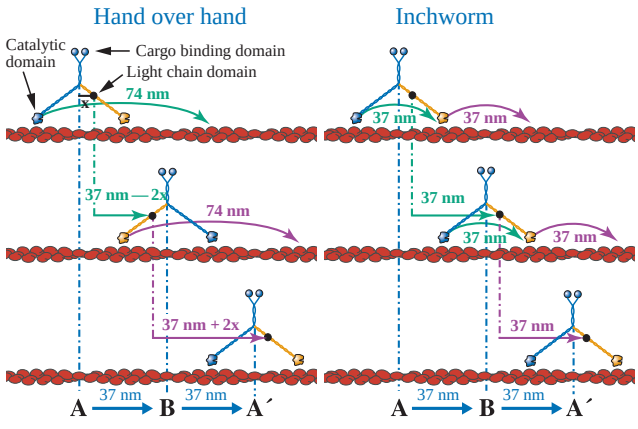

Fig. 1. Hand-over-hand versus inchworm model of myosin V motility. A calmodulin light chain is labeled with a single fluorescent dye and exchanged into the myosin V light chain domain, where it binds in one of several possible positions (black dot, schematic representation of dye position). In the hand-over-hand model, the rear head moves 74-nm forward but the front head does not move, the stalk moves 37 nm, and the dye takes alternating 37 ± 2x nm steps. (If the dye is a different distance from the stalk in the forward versus rear light chain domains, due to asymmetry in the myosin V structure, then x is the average distance of the dye from the stalk.) In the inchworm model, all parts of the myosin move 37-nm forward, and one head always leads. Adapted with permission from (*32*).

[1]Center for Biophysics and Computational Biology, [2]Physics Department, University of Illinois, Urbana-Champaign, IL 61801, USA. [3]University of Pennsylvania, Pennsylvania Muscle Institute, Philadelphia, PA 19104, USA.

*To whom correspondence should be addressed. E-mail: selvin@uiuc.edu

curve-fitting the image [also called the point-spread function (PSF)] to a Gaussian function (*20*, *21*). The fundamental goal is to determine the center or mean value of the distribution, $\mu = (x_0, y_0)$, and its uncertainty, the standard error of the mean, σ_μ. By measuring the position before and after a step, the step size can be determined. The relation between σ_μ and the number of collected photons (N), the pixel size of the imaging detector (a), the standard deviation of the background (b, which includes background fluorescence noise and detector noise), and the width of the distribution (standard deviation, s_i, in direction i), was derived by Thompson *et al.* in two dimensions (*18*)

$$\sigma_{\mu,i} = \sqrt{\left(\frac{s_i^2}{N} + \frac{a^2/12}{N} + \frac{8\pi s_i^4 b^2}{a^2 N^2}\right)} \quad (1)$$

where the index i refers to the x or y direction. The first term (s_i^2/N) is the photon noise, the second term is the effect of finite pixel size of the detector, and the last term is the effect of background.

Cy3 DNA localization and nanometric steps. Control experiments were done to demonstrate the ability to localize an immobile dye. Figure 2A shows the PSF of several individual Cy3 dyes attached to a coverslip via a DNA-biotin-streptavidin linkage, immersed in an aqueous buffer, and imaged with objective-type TIRF with an integration time of 0.5 s (*14*). For the highlighted PSF, N = 14,200 photons, a = 86 nm, b = 11, s_y = 122 nm, s_x = 125 nm [the full-width at half-maximum (FWHM) of the distribution, $\Gamma_i = 2.354$; $s_i \approx 287$ nm]. On the basis of Eq. 1, the expected σ_μ is 1.24 nm in each direction. Photon noise only (first term, Eq. 1) leads to σ_μ = 1.02 nm, pixelation (second term, Eq. 1) increases σ_μ to 1.04 nm, and background noise (third term, Eq. 1) increases σ_μ to 1.24 nm, showing that photon noise is the dominant contributor to σ_μ. A two-dimensional (2D) Gaussian analysis (Fig. 2B) yields an excellent fit (r^2 = 0.994; χ^2_r = 1.48) (fig. S2), with σ_μ = 1.3 nm, in excellent agreement with the expected value.

In addition, conditions have been found in which the dye is extremely photostable, often lasting for 1 to 3 min, enabling hundreds of 0.5-s images to be acquired (fig. S1). The use of an oxygen-scavenging system containing glucose oxidase and catalase (*22*) was an essential component in this photostability. The oxygen scavenging is similar to that reported previously (*23*, *24*), although an exact comparison is not possible because essential details were not previously reported.

Under these conditions, the highlighted PSF lasted 50 s, or 100 images, before photobleaching in a single step, for a total of ~1.4 million collected photons (fig. S1). We measured the center position of the PSF in each image and calculated the standard deviation for the 100 images. This should equal σ_μ of one PSF image if there is no drift or systematic error. We found the standard deviation is 1.46 nm, showing that the positional change of our system due to thermal fluctuations and vibrations is less than a nanometer and does not significantly affect our measurements on the "several minutes" time scale.

We then horizontally moved the coverslip containing the Cy3-DNA molecules via a nanometric stage in user-defined increments to test our ability to accurately and precisely measure step sizes. Figure 2, C and D, show measurements of 30 nm and <8 nm steps, with either a constant dwell time between steps or an exponentially distributed dwell time between steps. The latter is expected for a biomolecular motor that takes a step upon interaction with diffusing ATP. The precision is better than 1.3 nm, and the accuracy, determined by comparison to a calibrated stage, is better than 1 nm (*14*). Similar quality results were also achieved with 12-nm steps (fig. S3).

Step sizes of myosin V head. Next, we labeled myosin V on the light chain domain of the head (Fig. 1) with a single bifunctional rhodamine [bisiodoacetamidorhodamine (BR)] (*6*, *25*) or with monofunctional Cy3 (*26*). The labeled myosin V was added to F-actin filaments immobilized on a coverslip and observed using TIRF. Fluorescent images were collected with 0.5-s integration time. Roughly 20 individual spots, corresponding to different myosin V's, were observed per 40 μm by 40 μm area. Each had a FWHM of ≈280 nm. Approximately 5,000 to 10,000 photons per spot per image were collected, enabling us to locate the center to within ± 3 nm typically, and, for brighter spots, ± 1.5 nm. Some variation in intensity due to dye blinking was observed (Movie S1). After many images were analyzed, we found that the vast majority

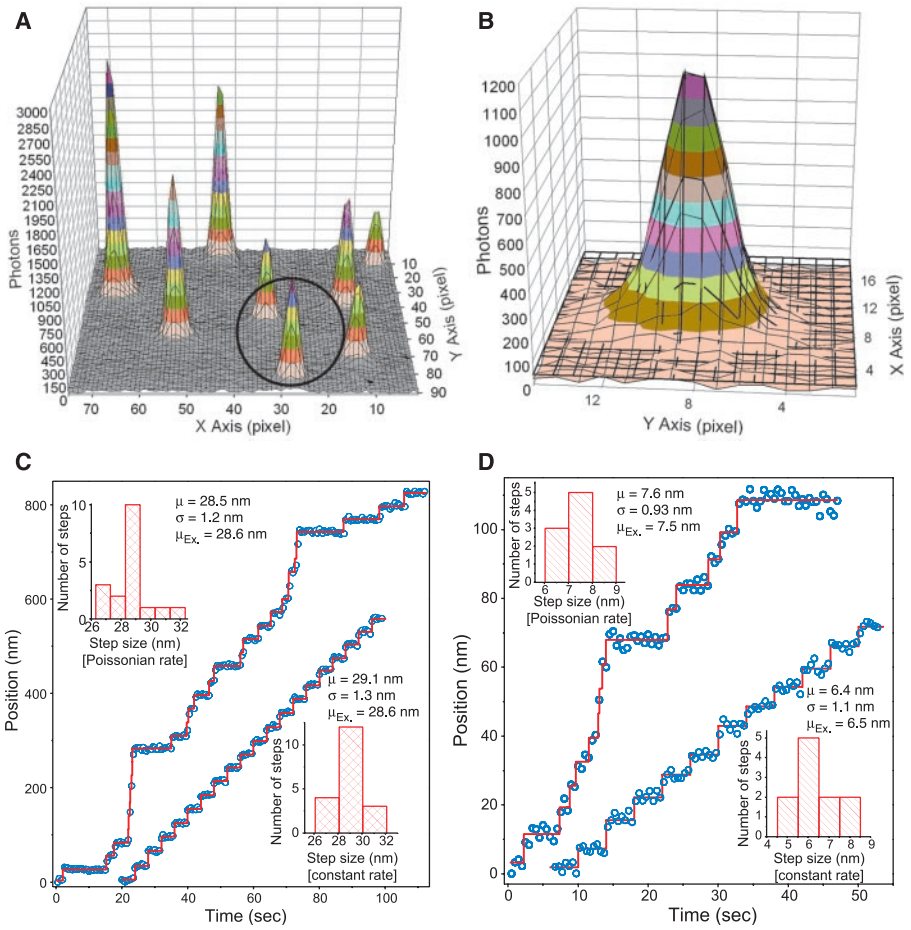

Fig. 2. PSF with 0.5-s integration time of several individual Cy3-dyes attached to a coverslip. (**A**) The intensity of each peak varies due to nonuniform illumination. (**B**) A Gaussian curve-fit (solid lines) to the PSF circled in (A) fits the PSF very well (r^2 =0.994), enabling the center to be determined to 1.3 nm. The width of the PSF is 287 nm, and the SNR is 32 at the pixel with maximum intensity (I_0 photons): SNR = $I_0/\sqrt{I_0+b^2}$; I_0 = 1134, b = 11. The fit contains small systematic errors due to the difference between a Gaussian and Airy function, leading to $\chi^2_r > 1$ (χ^2_r = 1.48) (*14*). The dye lasted for 100 images, or 50 s (fig. S1). Discernable 30-nm and ~7-nm steps are readily observed (**C** and **D**) upon moving the coverslip, either at a constant rate or a Poisson-distributed rate, with a nanometric stage and plotting the PSF center versus time. Red lines show the average position between each step. The precision (SD, σ, of the step size) is approximately 1 nm, and the accuracy [difference between the measured step size via PSF fitting (μ) and the expected step size (μ_{ex}) based on the calibrated stage] is better than 1 nm (*14*).

of spots displayed single quantal bleaching, indicative of a single molecule. Step sizes were analyzed only for singly labeled myosins.

In the absence of ATP, the fluorescent spots were immobile. The addition of ≈300 nM ATP led to discernable steps, and the average stepping rate increased with increasing ATP concentration. In total, we observed 49 different BR-labeled myosin V molecules and detected 552 total steps. We observed three different populations of myosin V molecules, exhibiting either uniform 74-nm steps, alternating 52- and 23-nm (52-23) steps, or alternating 42- and 33-nm (42-33) steps. Uniform 37-nm steps were not observed.

Specifically we detected 365 steps from 38 myosin V's, each of which stepped ≈ 74 nm (Fig. 3; Movie S1). Thirty-two of these molecules were bright enough to yield a signal-to-noise ratio (SNR) > 10 for a total of 231 steps. A histogram of these steps showed that the step size is 73.8 ± 5.3 nm (mean ± SD), with an excellent fit to a normal distribution (r^2 = 0.994, χ^2_r = 1.67) (Fig. 3). We also detected six molecules that took a total of 92 alternating 52-23 steps (Fig. 4), and six other molecules that took a total of 69 alternating 42-33 steps (Fig. 5). The histogram of the step size data shows three very distinct peaks for both the 52-23 and 42-33 data sets. For the 52-23 data, the averages of these peaks are 51.7 ± 4.1 nm, 23.1 ± 3.4 nm, and 73.6 ± 5.3 nm (mean ± SD). For the 42-33 data, the averages are 42.4 ± 2.9 nm, 32.8 ± 2.1 nm, and 74.1 ± 2.2 nm. The peak centered around 74 nm is consistent with myosin V molecules taking two steps (e.g., 52 nm + 23 nm = 75 nm) within 0.5 or 1 s, which could not be fully resolved because of the 0.5-s time resolution. The percentage of such missed steps is consistent with a probability distribution corresponding to exponentially distributed dwell times with an average step rate of 0.3 s^{-1} (Fig. 6).

When the myosin V was labeled with a Cy3-calmodulin, the observed step sizes were consistent with those measured with BR (Figs. 3 and 5). This acts as a control to ensure that the stepping characteristics we see are not specific to a particular dye. In particular, BR, which is attached by two points to the light chain, is highly polarized on the 0.5-s time scale (*6*), whereas Cy3, a monofunctional dye, is expected to have significantly lower polarization on this time scale and its residual orientation to be at a different angle with respect to the myosin than BR. For highly immobile single dyes, Bartko and Dickson (*27*) have shown that the PSF can take unusual shapes, including asymmetric ones, if spherical aberrations are present. However, the agreement between BR- and Cy3-labeled myosin V implies this is not a problem. Furthermore, in all cases, our PSFs are highly symmetric and are well fit by a Gaussian. This indicates that spherical aberrations are insignificant and that fluorophore orientation does not affect our ability to accurately measure translational motion.

These results strongly support a hand-over-hand model and are not consistent with an inchworm model. The hand-over-hand model predicts the dye will take alternating steps equal to the stalk-step-size ± 2x, and we interpret the uniform 74-nm steps arising from a dye attached to a light chain near the catalytic domain (stalk-step-size = 37 nm; x = 18.5 nm), perhaps on the first light chain. Using the same model, we interpret the 52-23 steps arising from a dye 6.5 to 7 nm from the midpoint in the direction of motion, probably corresponding to a dye on the fifth light chain, and the 42-33 steps arising from a dye 2 to 2.5 nm from the midpoint, probably corresponding to a dye on the sixth light chain (Fig. 1).

The hand-over-hand model predicts that for a dye very close to, or on, one catalytic domain, the steps will alternate between 74 nm and 0 nm (74-0) (Fig. 1). The 0-nm steps

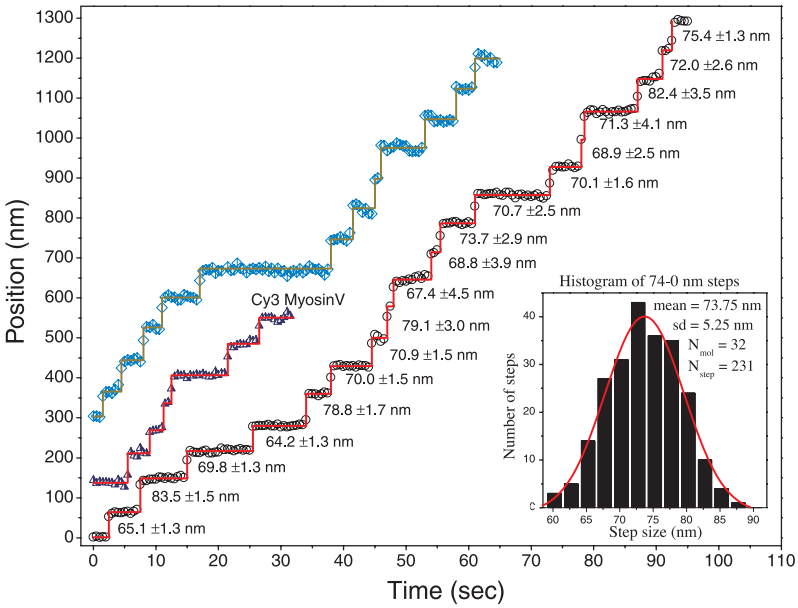

Fig. 3. Stepping traces of three different myosin V molecules displaying 74-nm steps and histogram (inset) of a total of 32 myosin V's taking 231 steps. Calculation of the standard deviation of step sizes can be found (*14*). Traces are for BR-labeled myosin V unless noted as Cy3 Myosin V. Lower right trace, see Movie S1.

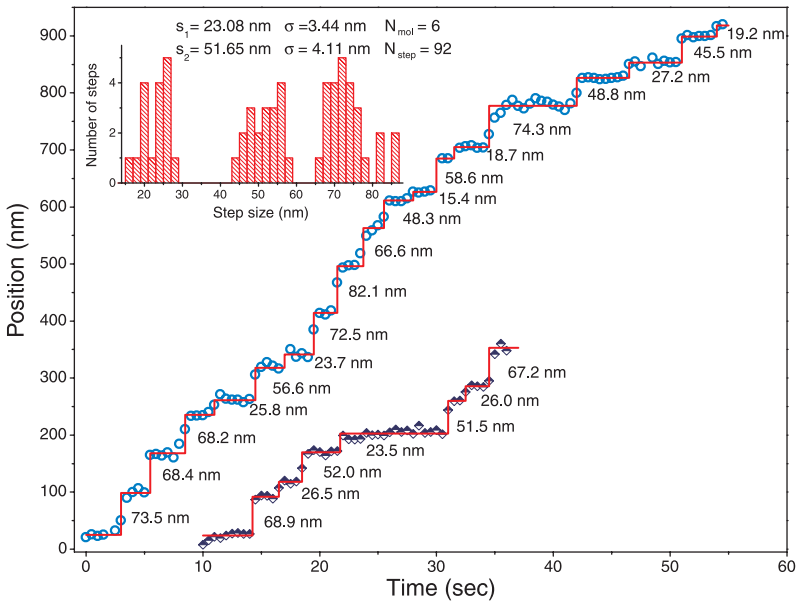

Fig. 4. Stepping traces of two different BR-labeled myosin V molecules displaying alternating 52-23 steps, and histogram of a total of six myosin V's taking 92 steps. Due to the 0.5-s time resolution of measurements, some steps are missed and yield 74-nm apparent steps, the sum of two steps. On the basis of the alternating step size, we infer that the dye is 7 nm from the center of mass along the direction of motion.

are not seen directly but can be inferred from a kinetic analysis of the stepping rate in two ways (Fig. 6). First, the apparent step rate for myosin V's displaying uniform 74-nm steps should be half that of the 42-33 or 52-23 steps at the same ATP concentration, because for every 74-nm step there is a hidden 0-nm step. This is indeed found: an average stepping rate of 0.35 s^{-1} for the myosins displaying 42-33 and 52-23 steps, and an average rate of 0.17 s^{-1} for the myosins displaying 74-nm steps.

Second, we can also detect the 0-nm steps indirectly via a kinetic analysis. If the step rate of one head is k_1 (A → B, Fig. 1) and the step rate of the other head is k_2 (B → A′, Fig. 1), then the dwell time probability distribution function for the A → B transition is $f(t) = k_1 e^{-k_1 t}$ and for the B → A′ transition is $g(t) = k_2 e^{-k_2 t}$. In the 42-33 and 52-23 cases, the total probability of dwell times is the sum of two exponentials: $P(t) = (k_1 e^{-k_1 t} + k_2 e^{-k_2 t})/2$. If each head has the same stepping rate, $P(t)$ reduces to a single exponential $P(t) = k_1 e^{-k_1 t}$. In the 74-nm case, the observable is A → A′, which is the convolution of two processes. If A → A′ takes t s, and A → B takes u s, then B → A′ will take $t - u$ s with $0 < u < t$. Integration over all possible values of u gives the convolution $P(t) = \int_0^t f(u) \cdot g(t-u)du = k_1 k_2 \cdot (e^{-k_1 t} - e^{-k_2 t})/(k_1 - k_2)$.

If the two rates are equal, then $P(t) = t k^2 e^{-kt}$. Note that $P(0) = 0$ and that $P(t)$ initially increases and then decreases for the 74-nm data if they contain hidden 0-nm steps, whereas the 42-33 or 52-23 data are expected to decay monotonically.

In Fig. 6, the histograms and theoretical fits show the expected convolution of two exponentials for alternating 74-0 steps and the exponential decay for the 42-33 and 52-23 steps; the histograms for the latter two are combined for improved statistics. The dwell time histogram of 74-nm steps fits well to a convolution with a single rate constant, $k = 0.328 \pm 0.007$ ($r^2 = 0.986$). Fitting to two different rate constants does not appreciably improve the curve fit (*28*). The histogram for the combined 42-33 and 52-23 steps was also well fit to a single rate constant, $k = 0.283 \pm 0.025$ ($r^2 = 0.984$). Fitting the dwell time histogram of the long (52 and 42) steps separately from the short (33 and 23) steps, the former gives a single rate constant of 0.25 ± 0.04 ($r^2 = 0.85$) and the latter gives a single rate constant of 0.32 ± 0.03 s^{-1} ($r^2 = 0.96$). Because these two rates are similar and because a single rate fits the combined data well, the stepping rates of the labeled and the unlabeled head are likely to be similar.

The above data were taken from multiple myosin V's observed simultaneously at the same ATP concentration ([ATP]) (300 nM). The resulting rates for the 74-0, 52-23, and 42-33 are in excellent agreement with each other and with expectations based on previously measured rate constants of ~0.3 s^{-1} at 300 nM ATP (*6*, *7*).

For the individual traces shown in the 74-0 data in Fig. 3, the fluctuations in step size are significantly larger than the uncertainties due to finite spatial resolution. For example, in the lower right trace of Fig. 3, the first step is 65.1 ± 1.3 nm and the second step is 83.5 ± 1.5 nm (*14*). The most straightforward interpretation is that the myoV is indeed taking different step sizes. The most likely step is 74 nm, corresponding to the two heads binding 13 actin monomers apart, but steps resulting in two heads separated by 11 and 15 monomers are also possible, leading to smaller or larger steps, respectively. Such a distribution of distances between bound heads has been observed by cryogenic electron microscopy (*29*).

Two other conclusions can be inferred from our data. The first is that the stalk-step-size is an average of 37 nm. This is inferred from the step size ± 2x analysis and from dividing the sum of two steps (74 + 0, 52 + 23, or 42 + 33 nm) by 2. Our 37-nm value is in good agreement with the 36 to 37 nm measured from the kinetics of calmodulin tilting rates (*6*) and the 40 nm measured in an optical trap (*30*), both of which were measured when actin was bound to a surface. The value is also similar to the 35 nm measured when actin was suspended above the surface (*9*, *10*). The second conclusion is that the dye in some myosin V molecules is located 18.5 nm from the center of mass along the direction of motion, which we infer from the 74-0 stepping pattern. This large distance can be explained by a "broken neck" model, in which the light chain

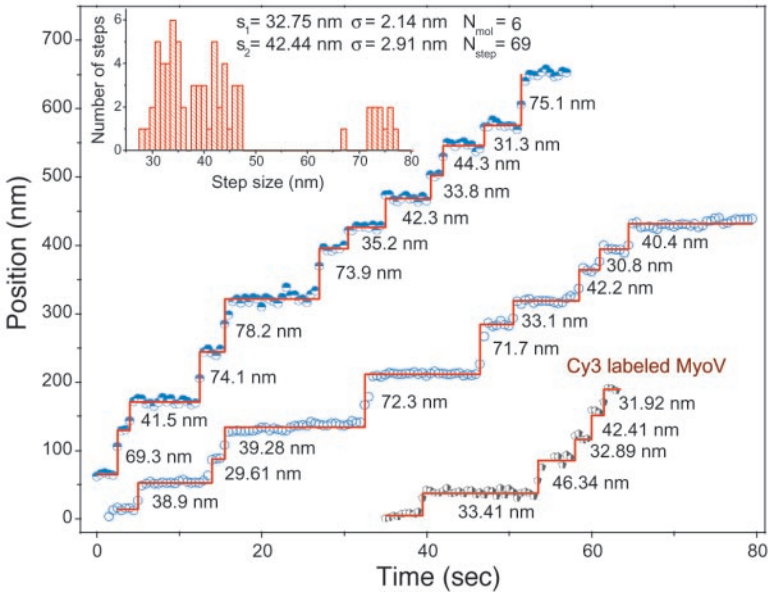

Fig. 5. Stepping traces of three different myosin V molecules displaying alternating 42-33 steps, and histogram of a total of six myosin V's taking 69 steps. These step sizes indicate that the dye is 2 to 3 nm from the center of mass along the direction of motion. The bottom right trace is for a Cy3-labeled myosin V, whereas the other two are for BR-labeled myosin V's. Due to the 0.5-s time resolution of measurements, some steps are missed and yield 74-nm apparent steps, the sum of two steps.

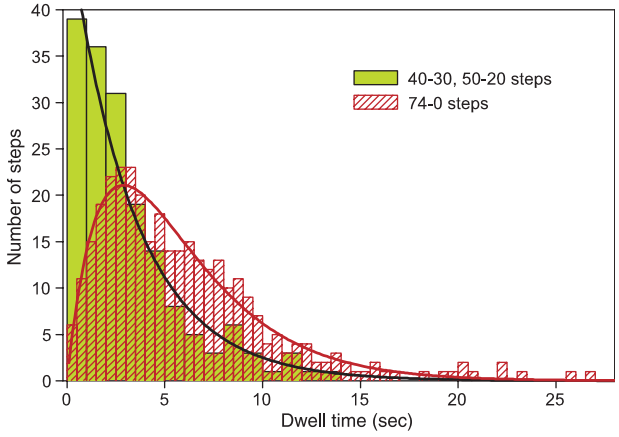

Fig. 6. Dwell time histograms for myosin V's displaying 74-nm steps (red cross-hatched, with solid red curve fit), or 52-23 and 42-33 combined (green with solid black curve fit). A 74-nm step in the 52-23 or 42-33 data (Figs. 4 and 5) is assumed to be two rapid steps (one dwell time) in the 0- to 0.5-s bin. The curve fits are based on the kinetic hand-over-hand model described in the text (Fig. 1) using a single rate constant for each histogram: $k_{52\text{-}23,42\text{-}23} = 0.28\ s^{-1}$; $k_{74\text{-}0} = 0.33\ s^{-1}$. A single rate constant is valid because the rate-limiting step is ATP binding at this low [ATP]; i.e., myosin V velocity is proportional to [ATP] (*6*). The rise at short times for the 74-nm data is indicative of a 0-nm intermediate step, i.e, 74-0-74-0 nm stepping sequence.

domain of the leading head is angled forward and has a kink shortly after emerging from the catalytic domain. This has been observed via electron microscopy (*29*), but is at odds with later work by the same group (*31*).

Conclusion. The specificity and sensitivity of single molecule fluorescence, combined with the nanometer spatial localization and enhanced photostability presented here, have enabled us to see step sizes of individual myosin V heads. The improvement in localization results from collecting a sufficiently high number of photons within the relevant time period (0.5 s) with high SNR, made possible by the high-efficiency, low-noise detector, and TIRF excitation minimizing background (*14*). Extended observation was possible through deoxygenation conditions that led to highly photostable dyes. Our results lead to the conclusion that myosin V moves in a hand-over-hand fashion, in agreement with the recent work of Forkey *et al.*, who measured tilting of BR-calmodulin in myosin V (*6*). Our conclusion is based on results at low [ATP] but likely holds at physiological [ATP] as well. Other tightly coupled motors, such as kinesin, may follow a similar scheme, and we now have the tools to examine this and other molecular motors.

Two types of hand-over-hand models have previously been proposed: an asymmetric model where each head is not functionally equivalent and where the stalk need not twist, and a symmetric model where each head is functionally equivalent and the stalk twists 180° on each step. Hua *et al.* found that the coiled-coil stalk of kinesin does not systematically twist as the motor steps (*8*), a result also reported for myosin V (*9*). Such asymmetric hand-over-hand models are attractive for cargo-carrying motors because they do not require a twisting of a large cargo or, conversely, a large torque that would tend to twist the motor. A definitive conclusion, however, between a symmetric and asymmetric hand-over-hand mechanism for myosin V—and perhaps other biomolecular motors—will need to await further experiments.

References and Notes

1. A. D. Mehta *et al.*, *Nature* **400**, 590 (1999).
2. C. Veigel, F. Wang, M. L. Bartoo, J. R. Sellers, J. E. Molloy, *Nature Cell Biol.* **4**, 59 (2002).
3. A. Mehta, *J. Cell Sci.* **114**, 1981 (2001).
4. S. L. Reck-Peterson, D. W. Provance Jr., M. S. Mooseker, J. A. Mercer, *Biochim. Biophys. Acta* **1496**, 36 (2000).
5. T. J. Purcell, C. Morris, J. A. Spudich, H. L. Sweeney, *Proc. Natl. Acad. Sci. U.S.A.* **99**, 14159 (2002).
6. J. N. Forkey, M. E. Quinlan, M. T. Shaw, J. E. Corrie, Y. E. Goldman, *Nature* **422**, 399 (2003).
7. E. M. De La Cruz, A. L. Wells, S. S. Rosenfeld, E. M. Ostap, H. L. Sweeney, *Proc. Natl. Acad. Sci. U.S.A.* **96**, 13726 (1999).
8. W. Hua, J. Chung, J. Gelles, *Science* **295**, 844 (2002).
9. M. Y. Ali *et al.*, *Nature Struct. Biol.* **9**, 464 (2002).
10. R. S. Rock *et al.*, *Proc. Natl. Acad. Sci. U.S.A.* **98**, 13655 (2001).
11. D. Axelrod, *Methods Cell Biol.* **30**, 245 (1989).
12. T. Funatsu, Y. Harada, M. Tokunaga, K. Saito, T. Yanagida, *Nature* **374**, 555 (1995).
13. M. Tokunaga, K. Kitamura, K. Saito, A. H. Iwane, T. Yanagida, *Biochem. Biophys. Res. Commun.* **235**, 47 (1997).
14. Materials and Methods are available as supporting online material on *Science* Online.
15. T. Schmidt, G. J. Schütz, W. Baumgartner, H. J. Gruber, H. Schindler, *Proc. Natl. Acad. Sci. U.S.A.* **93**, 2926 (1996).
16. U. Kubitscheck, O. Kückmann, T. Kues, R. Peters, *Biophys. J.* **78**, 2170 (2000).
17. T. D. Lacoste *et al.*, *Proc. Natl. Acad. Sci. U.S.A.* **97**, 9461 (2000).
18. R. E. Thompson, D. R. Larson, W. W. Webb, *Biophys. J.* **82**, 2775 (2002).
19. J. Gelles, B. J. Schnapp, M. P. Sheetz, *Nature* **331**, 450 (1988).
20. N. Bobroff, *Rev. Sci. Inst.* **57**, 1152 (1986).
21. M. K. Cheezum, W. F. Walker, W. H. Guilford, *Biophys. J.* **81**, 2378 (2001).
22. Y. Harada, K. Sakurada, T. Aoki, D. D. Thomas, T. Yanagida, *J. Mol. Biol.* **216**, 49 (1990).
23. K. Adachi *et al.*, *Proc. Natl. Acad. Sci. U.S.A.* **97**, 7243 (2000).
24. Y. Sambongi *et al.*, *Science* **286**, 1722 (1999).
25. J. E. T. Corrie *et al.*, *Nature* **400**, 425 (1999).
26. T. Sakamoto, I. Amitani, E. Yokota, T. Ando, *Biochem. Biophys. Res. Commun.* **272**, 586 (2000).
27. A. P. Bartko, R. M. Dickson, *J. Phys. Chem. B* **103**, 3053 (1999).
28. Fitting the data to two rate constants does not improve the fit; however, the curve is fit equally well to a range of (k_1, k_2), where k_1 and k_2 can differ by a factor of 2 or more. Hence, we cannot rule out asymmetry in the rates of the two heads.
29. M. L. Walker *et al.*, *Nature* **405**, 804 (2000).
30. M. Rief *et al.*, *Proc. Natl. Acad. Sci. U.S.A.* **97**, 9482 (2000).
31. S. Burgess *et al.*, *J. Cell Biol.* **159**, 983 (2002).
32. J. A. Spudich, *Nature Rev. Mol. Cell Biol.* **2**, 387 (2001).

33. Supported by NIH grants AR44420 (to P.R.S.), GM65367 (to T.H.), and AR26846 (to Y.E.G.); NSF grants DBI-02-15869 (to P.R.S. and T.H.) and 9984841 (to P.R.S.); the Carver Trust Foundation (to P.R.S.); and the DOE, Division of Materials Sciences (under award no. DEFG02-91ER45439), through the Frederick Seitz Materials Research Laboratory at the University of Illinois at Urbana-Champaign (to P.R.S.). S.A.M. was supported by a National Research Service Award in Molecular Biophysics (through NIH training grant PHS 5 T32 GM08276). We thank J. E. T. Corrie for gift of bis-rhodamine, E. Gratton for initial suggestions and discussions, B. C. Stevens for computer programming assistance, and I. Rasnik for fluorescence imaging assistance.

Supporting Online Material

www.sciencemag.org/cgi/content/full/1084398/DC1
Materials and Methods
Figs. S1 to S3
Movie S1
References

11 March 2003; accepted 21 May 2003
Published online 5 June 2003;
10.1126/science.1084398
Include this information when citing this paper.

Antibody Domain Exchange Is an Immunological Solution to Carbohydrate Cluster Recognition

Daniel A. Calarese,[1] Christopher N. Scanlan,[2,5] Michael B. Zwick,[2] Songpon Deechongkit,[3] Yusuke Mimura,[5] Renate Kunert,[6] Ping Zhu,[7] Mark R. Wormald,[5] Robyn L. Stanfield,[1] Kenneth H. Roux,[7] Jeffery W. Kelly,[3,4] Pauline M. Rudd,[5] Raymond A. Dwek,[5] Hermann Katinger,[6] Dennis R. Burton,[1,2*] Ian A. Wilson[1,4*]

Human antibody 2G12 neutralizes a broad range of human immunodeficiency virus type 1 (HIV-1) isolates by binding an unusually dense cluster of carbohydrate moieties on the "silent" face of the gp120 envelope glycoprotein. Crystal structures of Fab 2G12 and its complexes with the disaccharide Manα1-2Man and with the oligosaccharide $Man_9GlcNAc_2$ revealed that two Fabs assemble into an interlocked V_H domain-swapped dimer. Further biochemical, biophysical, and mutagenesis data strongly support a Fab-dimerized antibody as the prevalent form that recognizes gp120. The extraordinary configuration of this antibody provides an extended surface, with newly described binding sites, for multivalent interaction with a conserved cluster of oligomannose type sugars on the surface of gp120. The unique interdigitation of Fab domains within an antibody uncovers a previously unappreciated mechanism for high-affinity recognition of carbohydrate or other repeating epitopes on cell or microbial surfaces.

Neutralizing antibodies are elicited by most, if not all, successful vaccines (*1*, *2*). However, immunogens that are able to elicit neutralizing antibodies to a broad range of primary HIV-1 isolates have not been found. Nevertheless, a few rare, broadly neutralizing monoclonal antibodies that have been isolated from patients protect against viral challenge in animal models (*3*). Their epitopes include regions on gp41 [2F5 (*4*–*6*) and 4E10 (*6*, *7*)], the CD4-binding site of gp120 [b12 (*8*–*10*)], and part of the carbohydrate-masked "silent" face of gp120 [2G12 (*11*, *12*)]. A molecular understanding of the binding of these broadly neutralizing antibodies to their cognate envelope epitopes should facilitate rational HIV-1 vaccine design.

In this research article, we focus on the broadly neutralizing human antibody 2G12, which binds with nanomolar affinity to gp120. This antibody recognizes terminal